First-principles quantitative prediction of the lattice thermal conductivity in random semiconductor alloys: The role of force-constant disorder

Marco Arrigoni,[1,*] Jesús Carrete,[1] Natalio Mingo,[2] and Georg K. H. Madsen[1]
[1]*Institute of Materials Chemistry, TU Wien, A-1060 Vienna, Austria*
[2]*CEA, LITEN, 17 rue des Martyrs, F-38054 Grenoble, France*

(Received 11 December 2017; revised manuscript received 3 September 2018; published 25 September 2018)

The standard theoretical understanding of the lattice thermal conductivity κ_ℓ of semiconductor alloys assumes that mass disorder is the most important source of phonon scattering. In contrast, we find that for the random alloy $In_{1-x}Ga_xAs$ the hitherto neglected contribution of interatomic force-constant (IFC) disorder is essential for the prediction of κ_ℓ. We present an *ab initio* method based on special quasirandom structures and Green's functions which includes the role of IFC disorder and apply it in order to calculate κ_ℓ of $In_{1-x}Ga_xAs$ and $Si_{1-x}Ge_x$ alloys. We show that, while for $Si_{1-x}Ge_x$, phonon-alloy scattering is dominated by mass disorder, for $In_{1-x}Ga_xAs$, the inclusion of IFC disorder is fundamental to reproduce the experimentally observed κ_ℓ. We relate this to the underlying atomic-scale structural disorder in $In_{1-x}Ga_xAs$. This feature is common to most III-V and II-VI random semiconductor alloys, and we expect the inclusion of IFC disorder in modeling lattice thermal conductivity to be important for a wide class of materials.

DOI: 10.1103/PhysRevB.98.115205

I. INTRODUCTION

Random semiconductor alloys are receiving a considerable amount of attention due to their central role in a wide range of technologies, such as photonics [1,2], electronics, and optoelectronics [3–5]. It has been observed that important physical quantities, such as the lattice parameters and electronic band gap, can be made to vary continuously between the limiting values of the parent compounds [6], making the possibility of tuning the alloy properties through the component concentrations of particular interest.

The determination of the thermal conductivity κ is an essential part for the design of all power-dissipating devices, such as lasers, diodes, and transistors, based on these alloys. The ability to accurately calculate κ from first principles is, therefore, particularly attractive, as it can significantly help the discovery and design of materials with desirable thermal properties. In the last decade, the combination of density functional theory (DFT) with the Boltzmann transport equation (BTE) has proved to be a reliable method for accurately determining κ of many semiconductor and insulator materials. In these systems, phonons are the main heat carriers, and the principal contribution to κ is the lattice thermal conductivity κ_ℓ, which can be obtained from the *ab initio* computation of interatomic force constants [7,8]. While methods based on this approach are nowadays well established for calculating the κ_ℓ of single crystals [9–13] and are showing promising results for crystals with pointlike and extended defects [14–19], a method able to correctly describe κ_ℓ of general random semiconductor alloys is still missing. Currently, the most commonly employed approach is based on the virtual-crystal approximation (VCA) [20]. It consists of describing the random alloy by an effective medium whose properties [lattice constants, interatomic force constants (IFCs), masses, etc.] are given by the concentration average of the equivalent properties in the parent compounds. The thermal conductivity is then calculated from the averaged IFCs, and the effect of the alloy disorder on phonon transport is taken into account by introducing a mass perturbation in an approach analogous to the one employed by Tamura in the study of phonon scattering due to isotopic disorder [21]. This method has been successfully employed in calculating κ_ℓ of materials such as $Si_{1-x}Ge_x$ [22] and $Mg_2Si_{1-x}Sn_x$ [23]. However, it is not adequate to describe III-V and II-VI random semiconductor alloys, as one may see from the comparison between the VCA calculation for $In_{1-x}Ga_xAs$ [24] and the corresponding experimental values [25,26]. This lack of success can be linked to the primary hypothesis of the VCA, namely, the representation of an alloy through a nonstructural effective medium. In this medium, alloy atoms are placed in the exact same environment as they have in the parent compounds, and bond distances are simply assumed to depend linearly on the alloy concentration. In contrast, experimental observations have found that the atomic-scale structure of semiconductor alloys is actually characterized by large fluctuations from the average-medium structure of the VCA [6]. The presence of this structural disorder at the atomic scale will greatly affect the material's IFCs in a way that cannot be modeled by simply averaging over the pure-compound ones.

A rigorous treatment of the IFC disorder in random alloys is a long-lasting issue in the theoretical study of phonons in disordered systems [27]. The coherent potential approximation (CPA) is a single-site self-consistent approximation which was initially concerned with only mass disorder but was later generalized to include the IFC disorder in a simplified way [28–31]. An alternative approach is based on describing the alloy by a small cluster of atoms embedded

*marco.arrigoni@tuwien.ac.at

in an effective medium [32]. Such an approach was applied to study the phonon density of states of the mass-disordered linear chain [33], where it was found to yield more accurate results than the CPA. A detailed review of the application of such approximations to the phonon problem is given by Elliott *et al.* [34] and Dow *et al.* [35]. More recently, rigorous techniques able to take into account the off-diagonal disorder brought by the IFCs have been developed. These are based on the augmented-space formalism [36] and employ either a recursive method [37] or multiple-scattering theory [38]. Both have shown that the inclusion of the IFC disorder is essential for an accurate reproduction of the phonon dispersion relations of binary metal alloys characterized by IFCs which strongly differ between the parent compounds. Such approaches have also been used recently in combination with first-principles calculations and have shown a high predictive power [39,40]. Molecular dynamics has also been proposed as an alternative approach for semiconductor alloys coupled with the Green-Kubo modal analysis approach [41]. While in principle applicable with first-principles calculations [41], the method until now was based on empirical potentials, thereby limiting its predictive power.

Notwithstanding the progress in the theoretical description of lattice vibrations in random alloys, the first-principles determination of κ_l within the BTE is still mainly limited to the VCA. The main aim of this study is to extend the VCA in order to take into account the effect of the IFC disorder on the phonon elastic scattering processes. Details about the approximation employed in this study are given in Sec. II B; in brief, we employ a simplified approach related to the embedded-cluster approximation [32,33], in which the alloy is described by a finite number of atoms and an effective medium. In contrast to the embedded-cluster approximation, where the effective medium is described by the self-consistent CPA Green's function, in our approach the medium resembles the one given by the VCA. Furthermore, each atom in the alloy is considered an independent scatterer to which we relate an effective perturbation obtained from averaging the local perturbations associated with atoms of a given chemical species. We show that such an approach allows us to directly take into account the effect of structural disorder, through the inclusion of IFC perturbations, in a way which is both computationally simple, compared to the augmented-space-based approaches, and compatible with the existent DFT-BTE formalism.

We take cubic $In_{1-x}Ga_xAs$ as a model material as it can be considered a prototype system of a random alloy with an atomic-scale structure that significantly deviates from the VCA description. Homogeneous samples produced as ingots and bulk crystals are found to be random at any composition [42]. At the same time, extended x-ray-absorption fine-structure (EXAFS) measurements clearly show that the Ga-As and In-As nearest-neighbor (NN) distances in $In_{1-x}Ga_xAs$ are only weakly affected by the alloy concentration and assume values similar to those in the parent compounds [43]. As a result, the As-As NN distances show a bimodal distribution, while cation-cation distances, which agree better with the VCA, are still distributed over a somewhat broad range [43]. The presence of such structural disorder at the atomic scale is not unique to $In_{1-x}Ga_xAs$ but is observed in most III-V and II-VI random semiconductor alloys [6].

We show that by directly taking into account the local atomic-scale structural disorder a big improvement over the VCA can be achieved. The room-temperature experimentally observed κ_ℓ of $In_{1-x}Ga_xAs$ random alloys is reproduced within a relative error of around 10%, which is an accuracy comparable to the best predictions achieved for single crystals. On the other hand, we also show that in $Si_{1-x}Ge_x$ random alloys, the IFC disorder does not have a relevant effect on the phonon-alloy elastic scattering rates, which explains why nonstructural models such as the VCA are adequate for this compound.

II. THEORETICAL FRAMEWORK

A. Lattice thermal conductivity

The components of the lattice thermal conductivity tensor $\boldsymbol{\kappa}_\ell$ can be obtained from the solution of the BTE in the relaxation-time approximation as

$$\kappa_\ell^{\alpha\beta} = \frac{1}{k_B T^2 V} \sum_{\mathbf{q},p} n_0(n_0+1)(\hbar\omega_{\mathbf{q},p})^2 v^\alpha_{\mathbf{q},p} v^\beta_{\mathbf{q},p} \tau_{\mathbf{q},p}, \quad (1)$$

where α and β range over the Cartesian coordinates, $\mathbf{q}$ and p represent the phonon wave vector and branch, respectively, k_B is the Boltzmann constant, T is the temperature, V is the system unit cell volume, n_0 is the Bose-Einstein distribution, ω and $\mathbf{v}$ are the phonon angular frequency and group velocity, respectively, and τ is the relaxation time [7,8]. For a given system, the scattering rates $\tau^{-1}_{\mathbf{q},p}$ can be expressed as the sum of the scattering rates arising from the relevant scattering mechanisms (Matthiessen's rule). In the case of bulk semiconductor alloys at around room temperature, the most relevant scattering processes involve the three-phonon inelastic scattering and the elastic scattering with the alloy disorder. We can therefore express τ^{-1} as

$$\tau^{-1} = \tau^{-1}_{3p} + \tau^{-1}_{dis}, \quad (2)$$

where τ^{-1}_{3p} and τ^{-1}_{dis} represent the rates arising from the above-mentioned inelastic and elastic scattering processes, respectively.

We calculate the three-phonon scattering rates for the alloys in the VCA from the third-order IFC of the parent compounds, as described in Refs. [7,8]. This assumes that the anharmonicity of the disordered alloy can be approximated by that of the effective medium. Such approximation does not seem so severe, as one would expect the configuration average of the third-order IFC of the disorder system to resemble, as a first approximation, that of the effective medium. In the present study we show that this is indeed the case for second-order IFCs. Furthermore, such an approximation is, in any case, necessary, as the computational cost involved in calculating the third-order IFCs in disordered systems is prohibitive.

The next sections explain how the τ^{-1}_{dis} term is calculated in the present study.

B. Scattering due to disorder

The main difficulty in calculating κ_ℓ of random alloys is the evaluation of the elastic scattering rates $\tau_{\rm dis}^{-1}$, which entails the theoretical description of the vibrational properties of random alloys.

We start by considering the harmonic description of an ideal crystal. Suppose we are considering a finite portion of the crystal made of N_c primitive cells, each one containing r atoms, whose masses are indicated by $M^0(\eta)$, with $\eta = 0, 1, \ldots, r-1$. The crystal Hamiltonian in the harmonic approximation is

$$\mathbf{H}^0 = \sum_{l\eta\alpha} \frac{\mathbf{p}_\alpha(l\eta)}{2M^0(\eta)} + \frac{1}{2}\sum_{l\eta\alpha}\sum_{l'\eta'\beta} \Phi^0_{\alpha\beta}(l\eta; l'\eta')\mathbf{u}_\alpha(l\eta)\mathbf{u}_\beta(l'\eta'), \tag{3}$$

where l is an index used to label the lth primitive cell in the crystal, $\Phi^0_{\alpha\beta}(l\eta; l'\eta')$ is an element of the $3rN_c \times 3rN_c$ second-order IFC matrix, and $\mathbf{u}_\alpha(l\eta)$ is the operator describing the displacement from the equilibrium position of atom η in the primitive cell l along the Cartesian direction α. In matrix form, the equations of motion for this system can be written as [44]

$$(\mathbf{\Phi}^0 - \omega^2\mathbf{M}^0)\mathbf{u} = 0, \tag{4}$$

where $\mathbf{M}^0$ is the diagonal $3rN_c \times 3rN_c$ mass matrix. Equation (4) can be reduced to [44]

$$\mathbf{D}^0(\mathbf{q})\mathbf{e}_{\mathbf{q},p} = \omega^2_{\mathbf{q},p}\mathbf{e}_{\mathbf{q},p}, \tag{5}$$

where $\mathbf{D}^0(\mathbf{q})$ are the $3r \times 3r$ Fourier-transformed dynamical matrices.

Having solved the eigenvalue equation for the ideal crystal, we can calculate its Green's function $\mathbf{g}$, defined by [45]

$$(\omega^2\mathbf{I} - \mathbf{H}^0)\mathbf{g}(\omega^2) = \mathbf{I}. \tag{6}$$

Using the fact that $\mathbf{H}^0$ is a Hermitian matrix, we can define the system retarded Green's function $\mathbf{g}^+$ in terms of its eigenvalues and eigenvectors:

$$\mathbf{g}^+(\omega^2) = \lim_{\epsilon\to 0^+}\sum_{\mathbf{q},p}\frac{|\mathbf{q},p\rangle\langle\mathbf{q},p|}{\omega^2 - \omega^2_{\mathbf{q},p} + i\epsilon}, \tag{7}$$

where $|\mathbf{q},p\rangle$ is the representation of the back-transformed $\mathbf{e}_{\mathbf{q},p}$ in Dirac's notation.

Let us consider now the introduction of substitutional defects on the ideal crystal. We can write equations analogous to (3) and (4) for the defective crystal by simply substituting the ideal crystal masses $M^0(\eta)$ by the masses $M(l\eta)$ of defects replacing atoms η in the primitive cell l. Similarly, the presence of these defects will also change the system harmonic force constants, which entails the substitution of the elements of $\mathbf{\Phi}^0$ with those of a new IFC matrix $\mathbf{\Phi}$. The analog of Eq. (4) for the defective system is then

$$(\mathbf{\Phi} - \omega^2\mathbf{M})\mathbf{u} = 0, \tag{8}$$

which we rewrite as

$$\{(\mathbf{\Phi}^0 - \omega^2\mathbf{M}^0) + [\Delta\mathbf{\Phi} + \Delta\mathbf{M}(\omega^2)]\}\mathbf{u} = 0. \tag{9}$$

Equation (9) introduces the mass perturbation, $\Delta\mathbf{M}(\omega^2)$, and IFC perturbation, $\Delta\mathbf{\Phi}$, matrices, whose elements are given by

$$\Delta M_{\alpha\beta}(l\eta, l'\eta')(\omega^2) = -\omega^2[M(\eta) - M^0(\eta)]\delta_{ll'}\delta_{\eta\eta'}\delta_{\alpha\beta},$$
$$\Delta\Phi_{\alpha\beta}(l\eta, l'\eta') = \Phi_{\alpha\beta}(l\eta, l'\eta') - \Phi^0_{\alpha\beta}(l\eta, l'\eta'), \tag{10}$$

respectively. The influence on the ideal crystal equations of motion introduced by the substitutional impurities is therefore expressed through the introduction of the perturbation $\mathbf{V} \equiv \Delta\mathbf{\Phi} + \Delta\mathbf{M}(\omega^2)$.

We can now write the retarded Green's function of the perturbed crystal $\mathbf{G}^+$ in terms of this perturbation and the retarded Green's function of the ideal crystal as [45]

$$\mathbf{G}^+ = \mathbf{g}^+ + \mathbf{g}^+\mathbf{V}\mathbf{G}^+, \tag{11}$$

which can be expanded in a Born series,

$$\mathbf{G}^+ = \mathbf{g}^+ + \mathbf{g}^+\mathbf{V}\mathbf{g}^+ + \mathbf{g}^+\mathbf{V}\mathbf{g}^+\mathbf{V}\mathbf{g}^+ + \cdots, \tag{12}$$

and has the formal solution

$$\mathbf{G}^+ = (\mathbf{I} - \mathbf{g}^+\mathbf{V})^{-1}\mathbf{g}^+, \tag{13}$$

or in terms of the T matrix $\mathbf{T}^+ = (\mathbf{I} - \mathbf{V}\mathbf{g}^+)^{-1}\mathbf{V}$,

$$\mathbf{G}^+ = \mathbf{g}^+ + \mathbf{g}^+\mathbf{T}^+\mathbf{g}^+. \tag{14}$$

We consider now the case of a random alloy. To describe its vibrational properties we introduce an effective medium with the space-group symmetry of the parent compounds. Such a medium could, for example, be constructed employing the VCA or could be described by the CPA Green's function, as in the embedded-cluster approximation [33]. Within this picture, the actual alloy in a particular configuration σ can be seen as a perturbation on the effective medium. Therefore, we can then obtain the Green's function of the alloy in terms of the one of the effective medium $\mathbf{g}^+$ and the perturbation introduced by the alloy disorder. It is easy to see that all the steps involved are the same as those leading to Eq. (11), with the difference that now the perturbed Green's function is indexed by the particular alloy configuration: $\mathbf{G}^+(\sigma)$. The macroscopic properties of the random alloy are given by an average over all the possible configurations σ, and thus, one has to consider the averaged Green's function $\langle\mathbf{G}^+\rangle$ [34].

Obtaining the averaged Green's function is one of the main difficulties in the theoretical study of random alloys. We do not aim to rigorously perform the averaging but instead to find an approximate expression for the T matrix which is suitable for calculating $\tau_{\rm dis}^{-1}$. We start from Eq. (12) and perform the average on both sides to obtain

$$\langle\mathbf{G}^+\rangle = \mathbf{g}^+ + \mathbf{g}^+\langle\mathbf{V}\rangle\mathbf{g}^+ + \mathbf{g}^+\langle\mathbf{V}\mathbf{g}^+\mathbf{V}\rangle\mathbf{g}^+ + \cdots. \tag{15}$$

The Green's function of the effective medium $\mathbf{g}^+$ has been taken out of the average since it clearly does not depend on the particular alloy configuration. In a truly random alloy, the occupancy probabilities of the various atomic sites are statistically independent of one another. Based on this observation, in a single-site theory, $\langle\mathbf{G}^+\rangle$ of Eq. (15) could be

approximated as

$$\langle \mathbf{G}^+ \rangle \approx \mathbf{g}^+ + \mathbf{g}^+ \langle \mathbf{V} \rangle \mathbf{g}^+ + \mathbf{g}^+ \langle \mathbf{V} \rangle \mathbf{g}^+ \langle \mathbf{V} \rangle \mathbf{g}^+ + \cdots . \quad (16)$$

Therefore, assuming the Born series converges, we obtain

$$\langle \mathbf{G}^+ \rangle = (\mathbf{I} - \mathbf{g}^+ \langle \mathbf{V} \rangle)^{-1} \mathbf{g}^+ . \quad (17)$$

In such an approximation we identify an effective T matrix by

$$\mathbf{T}^+ = (\mathbf{I} - \langle \mathbf{V} \rangle \mathbf{g}^+)^{-1} \langle \mathbf{V} \rangle . \quad (18)$$

This T matrix can thus be obtained from the averaged perturbations and the Green's function of the effective medium. At this point, the elastic scattering rates can then be calculated from the imaginary part of the diagonal elements of the T matrix, employing the optical theorem, as explained in Ref. [46]:

$$\tau^{-1}_{\mathrm{dis},\mathbf{q},p} = -\frac{1}{\omega(\mathbf{q}, p)} \mathrm{Im}(\langle \mathbf{q}, p | \mathbf{T}^+ | \mathbf{q}, p \rangle). \quad (19)$$

Equations (18) and (19) describe the scattering between phonons and an effective averaged perturbation. Even though the equation was derived considering a single-site perturbation, as a first approximation, we assume that the same form of the effective T matrix can also be used to describe the scattering between phonons and a general perturbation with off-diagonal terms.

We are left with the problem of obtaining the IFC perturbation, for which a structural alloy model that allows the first-principles calculation of the IFCs of the disordered system is necessary. To this end, we employ special quasirandom structures (SQSs) [47]. These are supercells built in such a way that the correlation functions of a given set of atomic clusters (pairs, triplets, etc.) match those of a true random alloy as closely as possible. This approach, unlike nonstructural models, allows for a direct description of the local atomic structure and therefore for a quantitative evaluation of the effect of structural disorder on the system's IFCs. The use of SQSs in the first-principles DFT computation of second-order IFCs has been demonstrated in metallic alloys, where SQSs containing as few as 32 or 64 atoms allowed for accurate reproduction of the phonon band structure [39,40,48].

C. Effective medium

We now describe how the effective medium is constructed in the present study. Once the medium is defined, we can obtain its phonon properties such as the dispersion relations, group velocities, and the Green's function, necessary for the calculation of the lattice thermal conductivity given by Eq. (1).

As mentioned before, the effective medium could be constructed employing the VCA, i.e., by expressing the medium atomic masses, cell parameters, and IFCs as the concentration average of the respective quantities in the parent compounds. In practice, we did not use the concentration-averaged second-order IFCs, and thus, the effective medium used in this study is slightly different from the one defined by the VCA. However, taking $In_{0.3}Ga_{0.7}As$ as an explicit example, we demonstrate that the two media are essentially equivalent and the present treatment is not affected by the particular choice of the medium.

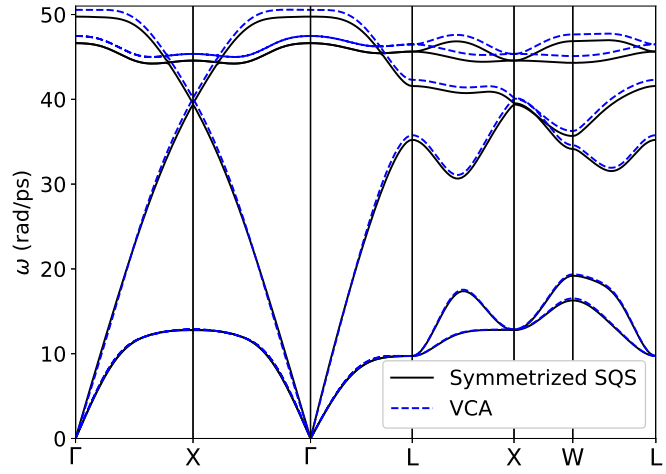

FIG. 1. Phonon band structure calculated for $In_{0.3}Ga_{0.7}As$ from the VCA force constants (dashed blue lines), compared with that obtained from the symmetrized SQS force constants (thick black lines). In both cases, the force constants were calculated using a $5 \times 5 \times 5$ supercell expansion of the zinc-blende primitive cell.

The second-order IFCs of our effective medium were obtained by symmetrizing the SQS IFCs according to the space-group symmetry of the parent compounds. This approach was chosen in order to use the same reference system (the SQS supercell) to calculate both Φ and Φ^0 of Eq. (10). The symmetrization procedure considers that the invariance of the IFCs with respect to the space-group operations entails that the IFC matrix element $\Phi_{\alpha\beta}(\eta, \eta')$ has to fulfill the condition

$$\Phi_{\alpha\beta}(\eta, \eta') = \frac{1}{|G|} \sum_{\mathbb{W} \in G} \sum_{\mu,\nu} W_{\alpha\mu} W_{\beta\nu} \Phi_{\mu\nu}\left(\mathbb{W}^{-1}(\eta); \mathbb{W}^{-1}(\eta')\right), \quad (20)$$

where $|G|$ is the order of the effective medium space group (whose translational subgroup is, however, limited to the translations enclosed in the supercell boundaries) and W is the linear part of the space group symmetry operation $\mathbb{W} \equiv \{W|\mathbf{w}\}$ (in Seitz notation) that moves the supercell atoms $\mathbb{W}^{-1}(\eta)$ and $\mathbb{W}^{-1}(\eta')$ into η and η', respectively. To simplify the notation, we condensed the two indexes $(l\eta)$ into a single index η running over all the rN_c atoms in the supercell. The acoustic sum rule and the symmetry of the IFC matrix are then self-consistently imposed.

Figure 1 shows a comparison between the phonon band structure of the effective medium, representing the $In_{0.3}Ga_{0.7}As$ random alloy, obtained through the VCA and through the symmetrization of the SQS IFCs.

D. Perturbation matrix and independent-scatterer approximation

The IFC perturbation is obtained as the difference between the "raw" SQS IFCs and the symmetrized ones, as described by Eq. (10). According to Eq. (15), $\langle \mathbf{V} \rangle$ should be obtained by averaging several different systems. In practice, the approximation leading to Eq. (16) implies that we can obtain $\langle \mathbf{V} \rangle$ from a single SQS.

To consider scattering processes consistent with the effective medium model, the perturbation must also be symmetrized. For the force-constant-related part of the perturbation $\Delta\mathbf{\Phi}$, we applied the same method outlined above, with the exception that in Eq. (20) the first sum runs over the symmetry operations belonging to the stabilizer of the crystallographic site where the scattering atom is located (in addition, the stabilizer order also replaces $|G|$). For example, in $In_{1-x}Ga_xAs$ the perturbation on the effective medium due to an In, Ga, or As atom is symmetrized employing the symmetry operations of the point group T_d.

We now apply the independent-scattering approximation in order to calculate the T matrix. Each scatterer in the system is considered independent (for $In_{1-x}Ga_xAs$ these scatterers are Ga, In, and As). Such an approach is computationally very simple, as it allows us to introduce a cutoff radius, which defines the cluster size, beyond which the perturbation induced by a given scatterer is considered to be zero. In practice we have found that the elastic scattering rates converge within a cutoff including the first five scatterer's neighbors, which considerably reduces the size of the matrices in Eq. (18).

Within our approximation, the perturbation averaging is essential in order to reproduce the experimental κ_ℓ of $In_{1-x}Ga_xAs$. For example, using a single $\mathbf{V}$ instead of $\langle\mathbf{V}\rangle$ in Eq. (18) tends to give a too low κ_ℓ: around 2 W m^{-1} K^{-1} compared to the experimental value of around 6 W m^{-1} K^{-1} for a GaAs concentration around 70%. This is not surprising, as in our approach the scattering between phonons and the alloy disorder is described through an effective average perturbation which reflects the underlying complex microscopic structure of the random alloy [34]. On the other hand, a compound containing a single impurity possesses an atomic-scale structure which is a very unlikely representative of the complex atomic configurations observed in random semiconductor alloys.

III. COMPUTATIONAL DETAILS

For both $In_{1-x}Ga_xAs$ and Si_xGe_{1-x} random alloys, the SQSs were generated from a $4 \times 4 \times 4$ supercell expansion of the zinc-blende primitive unit cell using the MCSQS module of the ALLOY THEORETICAL AUTOMATED TOOLKIT package [49]. For both materials, the parent compounds have closely related cubic structures (zinc blende for GaAs and InAs and diamond for Si and Ge) to a rhombohedral primitive cell containing two atoms. Therefore, the $4 \times 4 \times 4$ SQS contains a total of 128 atoms per supercell. In addition, SQSs with 250 atoms, corresponding to a $5 \times 5 \times 5$ expansion of the primitive cell, were considered for $In_{0.3}Ga_{0.7}As$ and $In_{0.75}Ga_{0.25}As$ in order to evaluate the convergence behavior with respect to the supercell size. For a given alloy concentration, SQSs were built considering the correlation function of clusters made of two, three, and four atoms, with interatomic distances up to the seventh-nearest-neighbor shells for couples and fourth-nearest-neighbor shells for triplets and quadruplets. The largest mismatch between the correlation functions of the fully random alloy and the SQSs was approximately 20% for the triplet correlation function in a single SQS.

All DFT calculations were carried out with the projector augmented-wave method [50] as implemented by the computational package VASP [51]. The vast majority of the calculations were done within the local-density approximation (LDA) [52]. In addition some calculations for $In_{0.3}Ga_{0.7}As$ and its parent compounds were performed employing the Perdew-Burke-Ernzerhof exchange-correlation functional revised for solids (PBEsol) [53]. For both functionals, a cutoff of the plane-wave energy of 500 eV was used, and the electronic structure was considered to be converged if the electronic energy changed from the previous loop in the self-consistent cycle by less than 10^{-8} eV. The supercell cell parameters were fixed according to Vegard's law. The ion positions in the supercell were relaxed until the net force experienced by each atom was less that 10^{-5} eV Å^{-1}. For LDA calculations, for the parent compounds of $In_{1-x}Ga_xAs$ and Si_xGe_{1-x} information about unit cell structure, second- and third-order IFCs, and, when necessary, Born effective charges and the dielectric tensor were taken from the online ALMABTE database [54].

Second-order IFCs were calculated for the SQS supercells by means of the finite-displacement method. The displacement creation and IFC extraction were carried out using the PHONOPY package [55]. A displacement of 0.01 Å was used in all LDA calculations. In PBEsol computations, both second- and third-order IFCs were calculated employing the finite-displacement method using a displacement amplitude of 0.03 Å for second-order IFCs and 0.05 Å for the third-order IFCs of the alloy parent compounds. The *ab initio* calculations for the SQS employed a reciprocal-space mesh which included only the Γ point. The only exception occurred for $In_{0.75}Ga_{0.25}As$, for which a finer mesh had to be used. The elastic and anharmonic scattering rates were calculated employing a fine incident phonon mesh of $32 \times 32 \times 32$ $\mathbf{q}$ points. The unperturbed Green's functions were calculated with the analytical tetrahedron method for reciprocal-space integration [56] employing a $25 \times 25 \times 25$ $\mathbf{q}$-point grid. All the modules needed for these operations were developed within the ALMABTE project [57].

IV. RESULTS

Figure 2 displays the bond length distributions obtained after relaxing the atomic positions in the SQSs representing

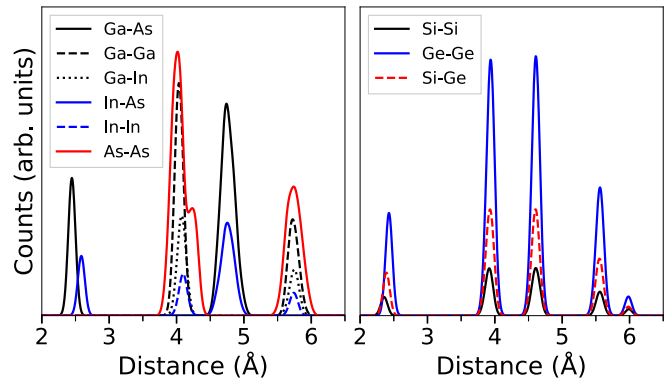

FIG. 2. Bond length distribution in $In_{0.3}Ga_{0.7}As$ (left) and $Si_{0.3}Ge_{0.7}$ (right) obtained from the atomic distances calculated with SQSs after applying a Gaussian broadening.

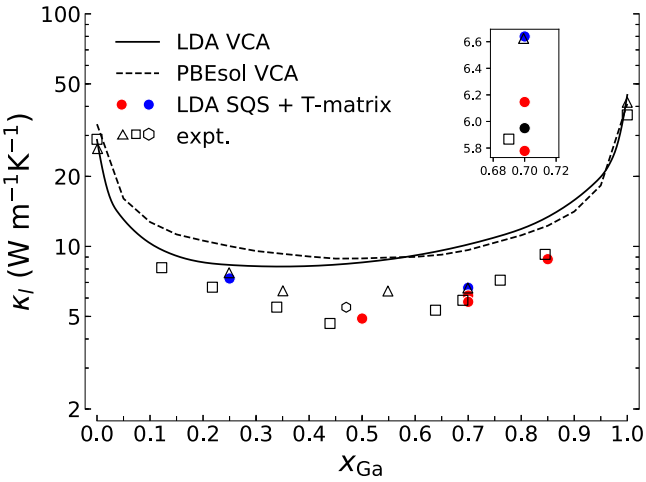

FIG. 3. Lattice thermal conductivity κ_ℓ of $In_{1-x}Ga_xAs$ calculated at 300 K from first principles with the VCA and with the improved approach based on SQSs. Solid red circles and blue circles represent values obtained using 128-atom and 250-atom SQSs, respectively. The solid black circle is obtained using the PBEsol functional. The experimental values obtained from Ref. [26] (open triangles), Ref. [25] (open squares), and Ref. [60] (open hexagon) are shown for comparison. For the $In_{0.3}Ga_{0.7}As$ composition, where the dependency of the results was tested for different supercell sizes, different SQS configurations, and two different functionals, the results are also shown as an inset using a linear scale for κ_ℓ.

$In_{0.3}Ga_{0.7}As$ and $Si_{0.3}Ge_{0.7}$ random alloys. As one can see, all the main features in the atomic-scale structure observed in the EXAFS experiments can be obtained from the SQS supercells. $In_{1-x}Ga_xAs$ NN distances show two distinct peaks, and fluctuations from the structure of the VCA medium are noticeable even beyond the first coordination shell. In particular, the presence of the experimentally observed [43] bimodal distribution of the As-As bond lengths is evident, and even if cation-cation and cation-anion bond distances beyond NNs show a single peak as the VCA predicts, their distribution is broader than in $Si_{1-x}Ge_x$. For $Si_{1-x}Ge_x$ we notice that the VCA structure is reproduced. Specifically, the NN distances possess a small tendency to a bimodal distribution, in agreement with experiments [58,59], but to a lesser degree than in $In_{1-x}Ga_xAs$. Bond distances beyond the NN ones are, on the other hand, concentrated around a single peak, independently of the chemical nature of the elements forming the bond.

To emphasize the role of the IFC disorder, we first calculated κ_ℓ for $In_{1-x}Ga_xAs$ using the VCA. The elastic scattering rates due to the alloy disorder $\tau_{\rm dis}^{-1}$ were obtained from Tamura's formula, which considers only the mass perturbation [21]. The calculated κ_ℓ in the VCA is shown in Fig. 3 by a thick black line (LDA) and a dashed line (PBEsol). It is evident that this approximation largely overestimates the measured value of κ_ℓ.

We then went beyond the mass perturbation picture and directly took into account the IFC disorder using the SQS supercell calculations and the Green's function perturbative treatment previously described. If not specifically stated, the calculations were done employing the LDA exchange-correlation functional, as only one alloy composition was considered with PBEsol for the sake of comparing the results given by two different functionals. We built several SQSs corresponding to different concentrations of $In_{1-x}Ga_xAs$ random alloys ($x = 0.25$, 0.5, 0.7, and 0.85) mostly in the Ga-rich region, where κ_ℓ predicted by the VCA in the LDA differs the most from the experiments. In particular, for $In_{0.3}Ga_{0.7}As$ we considered two different SQSs in order to evaluate to what extent the results are affected by the choice of the model system. As displayed in Fig. 3, the two different SQSs lead to values of κ_ℓ which differ by less than 0.4 W m^{-1} K^{-1}. In order to assess the effect of the exchange correlation functional on the value of κ_ℓ, we redid all the calculations for one of the SQSs of the composition $In_{0.3}Ga_{0.7}As$ using PBEsol. We obtained a value for κ_ℓ of 5.95 W m^{-1} K^{-1} (shown in the inset with a black dot), which is in good agreement with both the LDA and experimental values. Figure 3 also shows that employing 128-atom SQSs is already sufficient to obtain a value of κ_ℓ in very good agreement with the experimental data.

In the case of LDA calculations, one can notice that not only does the value of κ_ℓ calculated with the VCA quantitatively disagree with the experimental values and with the results of our calculations, but there is also a qualitative difference in the behavior of κ_ℓ with the alloy composition. From Fig. 3, one can see that, as InAs is characterized by a noticeably lower κ_ℓ than GaAs, the VCA predicts the minimum of κ_ℓ to be in the In-rich region, around $x_{\rm Ga} = 0.35$. This is not surprising as the predicted κ_ℓ of InAs is lower than that of GaAs (≈29 and ≈45 W m^{-1} K^{-1}, respectively). On the other hand, the experimental measurements and our calculations suggest that the minimum is located in the region where the In and Ga concentration in the alloy is around 50%. We note that in the case of PBEsol calculations, the minimum value is located in the same region found in the experiments. However, the predicted κ_ℓ still largely overestimates the experimental values. The discrepancy between LDA and PBEsol can be explained by considering that PBEsol gives a larger κ_ℓ than LDA for InAs (≈34 W m^{-1} K^{-1}) and a smaller one for GaAs (≈41 W m^{-1} K^{-1}), which shifts the VCA-predicted minimum from the In-rich region toward concentrations richer in Ga.

Finally, to emphasize the similarities and differences between our approach and the VCA, we also considered $Si_{1-x}Ge_x$ by building a single 128-atom SQS of $Si_{0.3}Ge_{0.7}$. For this compound differences in κ_ℓ between our method and the VCA amount to around 0.7 W m^{-1} K^{-1}, which is less than 10%. This difference stems from the different recipes used to calculate $\tau_{\rm dis}^{-1}$ due to the mass perturbation in the VCA and in our approach. For the former, we used Tamura's formula, which we noticed gives slightly larger values of $\tau_{\rm dis}^{-1}$ with respect to the values one obtains employing Eq. (19).

The different predictive power of the VCA between $In_{1-x}Ga_xAs$ and $Si_{1-x}Ge_x$ can be understood considering Fig. 4. The picture compares the values of $\tau_{\rm dis}^{-1}$, calculated with our method, in $In_{0.3}Ga_{0.7}As$ and $Si_{0.3}Ge_{0.7}$. The scattering rates are obtained considering the different terms in the expression $\langle \mathbf{V} \rangle = \langle \Delta \mathbf{M} + \Delta \mathbf{\Phi} \rangle$. We notice that for both compounds, for frequencies above 16 rad ps^{-1} ≈ 2.5 THz, the effect of the IFC disorder perturbation on the scattering rates is small, and the mass perturbation is the dominant term. For $Si_{1-x}Ge_x$, this is true also below 16 rad ps^{-1} except for a very

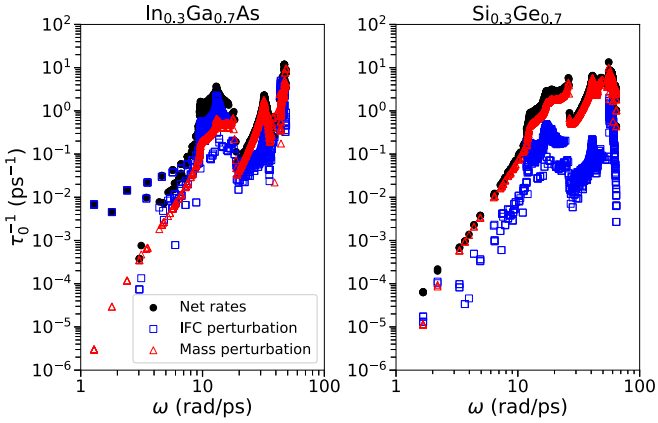

FIG. 4. Phonon-alloy elastic scattering rates calculated for $In_{0.3}Ga_{0.7}As$ (left) and $Si_{0.3}Ge_{0.7}$ (right) considering different types of perturbations: mass plus force-constant disorder (black solid circles), force-constant disorder (open blue squares), and mass disorder (open red triangles).

small region around 1 rad ps^{-1}, where the rates are close to zero in any case. On the other hand, $In_{1-x}Ga_xAs$ is characterized by the strong influence of the IFC disorder perturbation on τ_{dis}^{-1} below 16 rad ps^{-1}, corresponding to the region of the acoustic phonons frequencies. The effect of this phenomenon on κ_ℓ is particularly relevant since acoustic phonons are the main heat carriers in these systems. This fact emphasizes the inability of a simple mass perturbation to correctly describe alloy disorder in $In_{1-x}Ga_xAs$ and ultimately explains the failure of the VCA approach for this material. On the other hand, if the IFC disorder in the alloy is sufficiently small, the mass disorder will dominate the scattering processes, and the VCA gives reliable results, as is the case with $Si_{1-x}Ge_x$.

The source of the exceptionally strong phonon-alloy scattering found for $In_{1-x}Ga_xAs$ below 16 rad ps^{-1} partially originates from the polar nature of the system, as shown in Fig. 5. Here the elastic scattering rates are represented with different colors and symbols according to the phonon

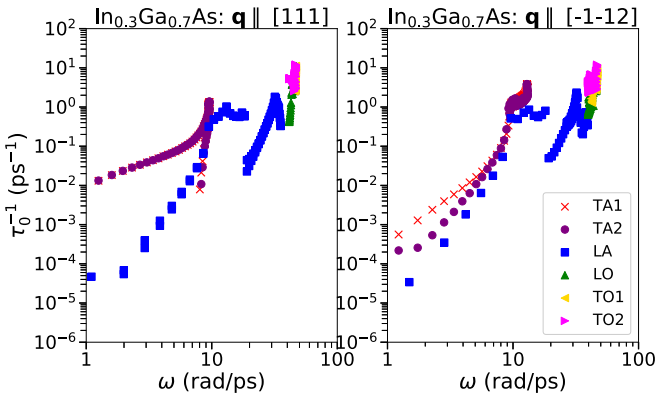

FIG. 5. Phonon-alloy elastic scattering rates calculated for $In_{0.3}Ga_{0.7}As$ for phonons with the wave vector parallel (left) or perpendicular (right) to the Ga/In-As NN dipole. TA, LA, TO, and LO indicate branches to which, respectively, transverse-acoustic, longitudinal-acoustic, transverse-optic, and longitudinal-optic phonons belong.

branch involved in the scattering process. On the left-hand side we depict incident phonons with the wave vector parallel to the [111] direction, along which lies the NN cation-anion dipole of the zinc-blende structure, and on the right-hand side we shown phonons with wave vectors along the $[-1, -1, 2]$ direction, which lies perpendicular to the [111] direction. When the phonon wave vector is parallel to the dipole, transverse-acoustic phonons (TA) are scattered much more strongly than longitudinal-acoustic (LA) ones, giving rise to the intense scattering rates shown in Fig. 4 for frequencies below 16 rad ps^{-1}. The dipole is, however, less perturbed by TA phonons traveling in a perpendicular direction, and the difference between the rates of TA and LA phonons is significantly smaller.

V. CONCLUSIONS

In conclusion, we have presented a general first-principles method for calculating κ_ℓ of random semiconductor alloys which includes the contribution of IFC disorder in the description of the alloy scattering events. We have shown that this inclusion is necessary in compounds such as $In_{1-x}Ga_xAs$, characterized by polar bonds and strong fluctuations of the atomic-scale structure from the one assumed in the VCA. On the other hand, in compounds such as $Si_{1-x}Ge_x$, where mass disorder is the leading factor, the VCA is a reasonable approximation. Overall, our method can be implemented with a reasonable amount of computational resources, is compatible with the existing phonon BTE formalism, and allows for the first-principles determination of κ_ℓ in general III-V and II-VI semiconductor alloys characterized by a random substitutional disorder.

The proposed method is introduced specifically for the study of truly random systems: The calculation of IFCs is carried out using SQSs which aim to represent a truly random disorder, and the approximations employed for the T matrix are based on a truly random occupation of lattice sites. However, we can assume that it might be extended to other systems in which the disorder in the IFCs plays an important role in the scattering of lattice vibrations. For example, epitaxial growth is known to lead to some degree of long-range order in certain semiconductor alloys [61,62]. We can generally expect that the presence of such order would affect the lattice thermal conductivity of the material. At the same time, the complex local atomic-scale structure characteristic of such alloys would still induce a strong disorder in the IFCs, creating an interplay between the short- and long-range structural features. Similarly, IFC disorder would still have important effects at interfaces, where the atomic structure is considerably more disordered than in the bulk, and can indeed affect the scattering of phonons in superlattices [63].

ACKNOWLEDGMENTS

We acknowledge support from the European Union's Horizon 2020 Research and Innovation Programme, Grant No. 645776 (ALMA). We thank the Vienna Scientific Cluster for providing the computational facilities (Project No. 70958: ALMA).

[1] R. Chen, T.-T. D. Tran, K. W. Ng, W. S. Ko, L. C. Chuang, F. G. Sedgwick, and C. Chang-Hasnain, Nat. Photonics **5**, 170 (2011).

[2] Y. Yao, A. J. Hoffman, and C. F. Gmachl, Nat. Photonics **6**, 432 (2012).

[3] S. Mokkapati and C. Jagadish, Mater. Today **12**, 22 (2009).

[4] S.-I. Park, A.-P. Le, J. Wu, Y. Huang, X. Li, and J. A. Rogers, Adv. Mater. **22**, 3062 (2010).

[5] M. A. Itzler, X. Jiang, M. Entwistle, K. Slomkowski, A. Tosi, F. Acerbi, F. Zappa, and S. Cova, J. Mod. Opt. **58**, 174 (2011).

[6] C. S. Schnohr, Appl. Phys. Rev. **2**, 031304 (2015).

[7] N. Mingo, D. Stewart, D. Broido, L. Lindsay, and W. Li, in *Length-Scale Dependent Phonon Interactions*, edited by S. Shindé and G. Srivastava (Springer, New York, 2014), Chap. 5, pp. 137–173.

[8] W. Li, J. Carrete, N. A. Katcho, and N. Mingo, Comput. Phys. Commun. **185**, 1747 (2014).

[9] D. A. Broido, M. Malorny, G. Birner, N. Mingo, and D. A. Stewart, Appl. Phys. Lett. **91**, 231922 (2007).

[10] A. Ward, D. A. Broido, D. A. Stewart, and G. Deinzer, Phys. Rev. B **80**, 125203 (2009).

[11] L. Lindsay, D. A. Broido, and T. L. Reinecke, Phys. Rev. Lett. **109**, 095901 (2012).

[12] J. Ma, W. Li, and X. Luo, Appl. Phys. Lett. **105**, 082103 (2014).

[13] B. Vermeersch, J. Carrete, N. Mingo, and A. Shakouri, Phys. Rev. B **91**, 085202 (2015).

[14] N. A. Katcho, J. Carrete, W. Li, and N. Mingo, Phys. Rev. B **90**, 094117 (2014).

[15] A. Katre, J. Carrete, and N. Mingo, J. Mater. Chem. A **4**, 15940 (2016).

[16] A. Katre, J. Carrete, B. Dongre, G. K. H. Madsen, and N. Mingo, Phys. Rev. Lett. **119**, 075902 (2017).

[17] T. Wang, J. Carrete, A. van Roekeghem, N. Mingo, and G. K. H. Madsen, Phys. Rev. B **95**, 245304 (2017).

[18] B. Dongre, J. Carrete, A. Katre, N. Mingo, and G. K. H. Madsen, J. Mater. Chem. C **6**, 4691 (2018).

[19] A. Katre, J. Carrete, T. Wang, G. K. H. Madsen, and N. Mingo, Phys. Rev. Mater. **2**, 050602 (2018).

[20] B. Abeles, Phys. Rev. **131**, 1906 (1963).

[21] S.-i. Tamura, Phys. Rev. B **27**, 858 (1983).

[22] J. Garg, N. Bonini, B. Kozinsky, and N. Marzari, Phys. Rev. Lett. **106**, 045901 (2011).

[23] W. Li, L. Lindsay, D. A. Broido, D. A. Stewart, and N. Mingo, Phys. Rev. B **86**, 174307 (2012).

[24] B. Vermeersch, J. Carrete, and N. Mingo, Appl. Phys. Lett. **108**, 193104 (2016).

[25] M. Abrahams, R. Braunstein, and F. Rosi, J. Phys. Chem. Solids **10**, 204 (1959).

[26] E. F. Hockings, I. Kudman, T. E. Seidel, C. M. Schmelz, and E. F. Steigmeier, J. Appl. Phys. **37**, 2879 (1966).

[27] P. Carruthers, Rev. Mod. Phys. **33**, 92 (1961).

[28] D. W. Taylor, Phys. Rev. **156**, 1017 (1967).

[29] T. Kaplan and M. Mostoller, Phys. Rev. B **9**, 353 (1974).

[30] G. Grünewald, J. Phys. F **6**, 999 (1976).

[31] T. Kaplan and L. J. Gray, Phys. Rev. B **14**, 3462 (1976).

[32] A. Gonis and J. W. Garland, Phys. Rev. B **16**, 2424 (1977).

[33] C. W. Myles and J. D. Dow, Phys. Rev. B **19**, 4939 (1979).

[34] R. J. Elliott, J. A. Krumhansl, and P. L. Leath, Rev. Mod. Phys. **46**, 465 (1974).

[35] J. D. Dow, W. E. Packard, H. A. Blackstead, and D. W. Jenkins, in *Phonon Physics: The Cutting Edge*, edited by G. Horton and A. Maradudin, Dynamical Properties of Solids Vol. 7 (North-Holland, Amsterdam, 1995), pp. 349–424.

[36] A. Mookerjee, J. Phys. C **6**, L205 (1973).

[37] A. Alam and A. Mookerjee, Phys. Rev. B **69**, 024205 (2004).

[38] S. Ghosh, P. L. Leath, and M. H. Cohen, Phys. Rev. B **66**, 214206 (2002).

[39] O. Grånäs, B. Dutta, S. Ghosh, and B. Sanyal, J. Phys.: Condens. Matter **24**, 015402 (2012).

[40] R. K. Chouhan, A. Alam, S. Ghosh, and A. Mookerjee, Phys. Rev. B **89**, 060201 (2014).

[41] H. R. Seyf, L. Yates, T. L. Bougher, S. Graham, B. A. Cola, T. Detchprohm, M.-H. Ji, J. Kim, R. Dupuis, W. Lv, and A. Henry, npj Comput. Mater. **3**, 49 (2017).

[42] J. C. Mikkelsen and J. B. Boyce, Phys. Rev. B **28**, 7130 (1983).

[43] J. C. Mikkelsen and J. B. Boyce, Phys. Rev. Lett. **49**, 1412 (1982).

[44] A. A. Maradudin and S. H. Vosko, Rev. Mod. Phys. **40**, 1 (1968).

[45] E. N. Economou, *Green's Functions in Quantum Physics* (Springer, Berlin, 2006).

[46] N. Mingo, K. Esfarjani, D. A. Broido, and D. A. Stewart, Phys. Rev. B **81**, 045408 (2010).

[47] A. Zunger, S.-H. Wei, L. G. Ferreira, and J. E. Bernard, Phys. Rev. Lett. **65**, 353 (1990).

[48] Y. Wang, C. L. Zacherl, S. Shang, L.-Q. Chen, and Z.-K. Liu, J. Phys.: Condens. Matter **23**, 485403 (2011).

[49] A. van de Walle, P. Tiwary, M. de Jong, D. Olmsted, M. Asta, A. Dick, D. Shin, Y. Wang, L.-Q. Chen, and Z.-K. Liu, CALPHAD: Comput. Coupling Phase Diagr **42**, 13 (2013).

[50] P. E. Blöchl, Phys. Rev. B **50**, 17953 (1994).

[51] G. Kresse and D. Joubert, Phys. Rev. B **59**, 1758 (1999).

[52] J. P. Perdew and A. Zunger, Phys. Rev. B **23**, 5048 (1981).

[53] G. I. Csonka, J. P. Perdew, A. Ruzsinszky, P. H. T. Philipsen, S. Lebègue, J. Paier, O. A. Vydrov, and J. G. Ángyán, Phys. Rev. B **79**, 155107 (2009).

[54] ALMABTE Database, http://www.almabte.eu/index.php/database/.

[55] A. Togo and I. Tanaka, Scr. Mater. **108**, 1 (2015).

[56] P. Lambin and J. P. Vigneron, Phys. Rev. B **29**, 3430 (1984).

[57] J. Carrete, B. Vermeersch, A. Katre, A. van Roekeghem, T. Wang, G. K. H. Madsen, and N. Mingo, Comput. Phys. Commun. **220**, 351 (2017).

[58] H. Kajiyama, S.-i. Muramatsu, T. Shimada, and Y. Nishino, Phys. Rev. B **45**, 14005 (1992).

[59] J. C. Aubry, T. Tyliszczak, A. P. Hitchcock, J.-M. Baribeau, and T. E. Jackman, Phys. Rev. B **59**, 12872 (1999).

[60] W. Kim, J. Zide, A. Gossard, D. Klenov, S. Stemmer, A. Shakouri, and A. Majumdar, Phys. Rev. Lett. **96**, 045901 (2006).

[61] T. S. Kuan, T. F. Kuech, W. I. Wang, and E. L. Wilkie, Phys. Rev. Lett. **54**, 201 (1985).

[62] G. Stringfellow, J. Cryst. Growth **98**, 108 (1989).

[63] S. P. Hepplestone and G. P. Srivastava, Phys. Rev. B **82**, 144303 (2010).